Emission of Pr^{3+} in $SrAl_{12}O_{19}$ under vacuum ultraviolet synchrotron excitation

2003 J. Phys.: Condens. Matter 15 719

(http://iopscience.iop.org/0953-8984/15/4/311)

INSTITUTE OF PHYSICS PUBLISHING JOURNAL OF PHYSICS: CONDENSED MATTER

J. Phys.: Condens. Matter **15** (2003) 719–729 PII: S0953-8984(03)55684-3

Emission of Pr^{3+} in $SrAl_{12}O_{19}$ under vacuum ultraviolet synchrotron excitation

P A Rodnyi[1], P Dorenbos[2,4], G B Stryganyuk[3], A S Voloshinovskii[3], A S Potapov[1] and C W E van Eijk[2]

[1] St Petersburg State Polytechnical University, Polytechnicheskaya 29, 195251, St Petersburg, Russia
[2] Delft University of Technology, Interfaculty Reactor Institute, Mekelweg 15, 2629 JB Delft, The Netherlands
[3] National University of Lviv, Kirilo i Mefodii 8, 290005 Lviv, Ukraine

Received 6 November 2002
Published 20 January 2003
Online at stacks.iop.org/JPhysCM/15/719

Abstract

$SrAl_{12}O_{19}$:Pr phosphors have been investigated under ultraviolet/vacuum ultraviolet (5–20 eV) synchrotron radiation at room and near liquid He temperatures. The excitation of $^1S_0 \rightarrow {}^1I_6$ and $^3P_0 \rightarrow {}^3H_4$ emission of Pr^{3+} in $SrAl_{12}O_{19}$ occurs in a 1 eV wide region originating from the interconfiguration $4f^2 \rightarrow 4f5d$ transitions with threshold (onset of the transitions) at 6.0 eV at room temperature and at 6.15 eV at 14 K. A comparison of the excitation spectra of Pr^{3+} and known data for Ce^{3+} in $SrAl_{12}O_{19}$ reveals a shift of 1.52 eV between 5d states of the ions. The next threshold near 7.5 eV corresponds to the transitions from valence to conduction band. The luminescence from the $^3P_0$ level is excited efficiently at low temperature while $^1S_0$ luminescence is absent under band-to-band excitation. To explain this, a mechanism involving valence hole trapping and energy transfer from excitonic states to Pr^{3+} is proposed. At excitation near the maximum of $4f^2 \rightarrow 4f5d$ transitions (6.4 eV), the $^1S_0 \rightarrow {}^1I_6$ luminescence exhibits exponential decay with constant $\tau = 330 \pm 10$ ns at 300 K and $\tau \approx 400$ ns at 14 K. At pre-threshold excitation ($E < 6.0$ eV) a fast component $\tau \approx 10$ ns originating from excitonic emission prevails.

1. Introduction

Strontium aluminate $SrAl_{12}O_{19}$ is a convenient host crystal for rare-earth and transition metal dopants. Polycrystalline $SrAl_{12}O_{19}$:Mn is known as a green-emitting phosphor for plasma display panels [1], and Pr- or Nd-doped $SrAl_{12}O_{19}$ crystals show good laser properties [2]. $SrAl_{12}O_{19}$ has the magnetoplumbite structure and belongs to the D^4_{6h} space group [3]. Strontium in the crystal has a large coordination number (12) and large distances to nearest-neighbour

[4] Author to whom any correspondence should be addressed.

oxygen ions (2.750–2.785 Å); as a result the dopant (Pr) encounters a rather weak crystal field [4, 5]. The upper $^1S_0$ state of the $4f^2$ configuration of Pr^{3+} ions in weak-crystal-field environments can lie below the lowest 4f5d state, making it possible to observe photon cascade emission (PCE). For a high energy of the 4f5d states it is important also that the oxygen ligands are strongly bonded to cations (Al) with large electronegativity. The large number of Al in $SrAl_{12}O_{19}$ provides this relatively strong bond [5].

$SrAl_{12}O_{19}$:Pr has been investigated as a promising phosphor possessing cascade emission [6–10]. The first step of the cascade corresponds to $^1S_0 \rightarrow {}^1I_6$ transitions of Pr^{3+} ions, while the second step involves $^3P_0 \rightarrow {}^3H_j$, ^3F_j transitions. The following properties of $SrAl_{12}O_{19}$:Pr have been studied: emission spectra [6, 8, 9], decay kinetics [6–8], the influence of temperature and Pr concentration on emission properties [8, 9], the mixing of the $^1S_0$, $4f^2$ state and some states of the 4f5d configuration of Pr^{3+} ions [10]. The emission from the $^3P_0$ level of Pr^{3+} in $SrAl_{12}O_{19}$ has been investigated in detail in [11].

Despite the extensive studies of $SrAl_{12}O_{19}$:Pr, some physical processes going on in the compound remain unclear, such as the mechanism of energy transfer from the host to the activator, the origin of the fast emission component of f–f transitions, and peculiarities of the excitation spectra. In the present work we continue the investigation of spectral and decay kinetics properties of $SrAl_{12}O_{19}$:Pr. Emission and excitation time-resolved spectra of the phosphor have been measured at room and near LHe temperature using vacuum ultraviolet (VUV) synchrotron radiation. The investigation allowed us to reveal some new properties of $SrAl_{12}O_{19}$:Pr and propose a mechanism of energy transfer from the host to the activator.

2. Experimental details

The $SrAl_{12}O_{19}$:Pr phosphors were synthesized by firing of thoroughly mixed batches of the corresponding oxides. The host matrices for the phosphors were prepared from chemically pure or high-purity reagents. Analytical-grade chemicals were used as activators, co-activators, and fluxes. The polycrystalline samples obtained were subjected to x-ray diffraction analysis, and only single-phase samples were used in further experiments. In fact we used the same set of the samples as in previous works [8, 9], i.e., $SrAl_{12}O_{19}$ containing 0.05, 0.1, 0.5, and 1.0% of Pr^{3+}. The appropriate amount of Mg^{2+} was introduced to the compounds on Al^{3+} sites that act as charge compensation for Pr^{3+} replacing Sr^{2+}.

The measurements were performed on the Deutsches Electronen Synchrotron (DESY) in Hamburg using the SUPERLUMI set-up at HASYLAB. Details on the excitation set-up can be found elsewhere [12]. Excitation spectra were recorded in the region from 5 to 20 eV with a typical resolution of 0.3 nm. The emission spectra were detected using a monochromator–PMT system (200–600 nm) with a resolution of about 1 nm. The emission and excitation spectra were measured in three regimes:

(1) the time-integrated spectrum, i.e., with no time gate;
(2) the 'slow' component of the spectrum with 100 ns delay and a 400 ns window; and
(3) the 'fast' component of the spectrum with a 5 ns window and without delay.

The measurements were carried out at 300 and 14 K. The temperature dependences of the luminescence intensities were measured under x-ray (40 kV, 15 mA) excitation.

3. Results

Figure 1 presents emission spectra of the $SrAl_{12}O_{19}$:Pr (1%) sample measured at 14 K and at 6.7 eV (185 nm) excitation. The energy levels of the $4f^2$ configuration of Pr^{3+} are well

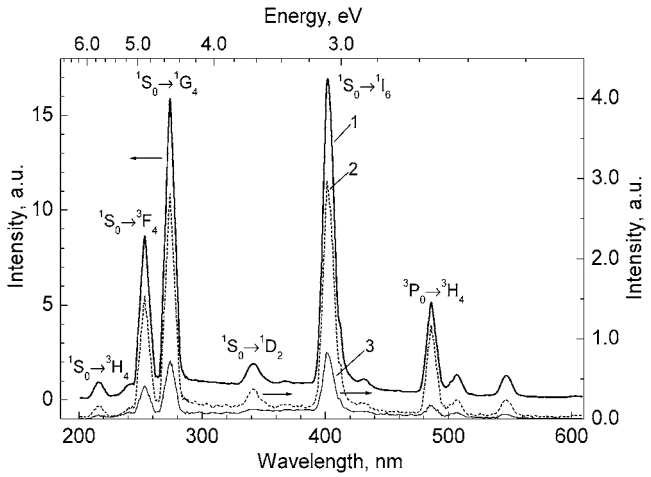

Figure 1. Emission spectra of $SrAl_{12}O_{19}$:Pr (1%) excited by 6.7 eV (185 nm) quanta: 1: time-integrated; 2: slow (100–500 ns); and 3: fast (0–5 ns) components. $T = 14$ K.

known and the origin of different lines can be easily established (see the designations in figure 1). The positions of the emission lines in the spectrum are quite similar to those at room temperature [6–8]. However, the intensities of the lines differ; in particular, two UV lines at 253.4 nm ($^1S_0 \rightarrow {}^3F_4$) and 273.6 nm ($^1S_0 \rightarrow {}^1G_4$) are relatively intense in the low-temperature spectrum. The slow spectrum (curve 2, figure 1) is very similar to the integral one (curve 1, figure 1). The contribution of the fast component (curve 3, figure 1) is smallest for $^1S_0 \rightarrow {}^3H_4$ and $^1S_0 \rightarrow {}^1D_2$ transitions. The most important lines are at 402 nm ($^1S_0 \rightarrow {}^1I_6$) and 486 nm ($^3P_0 \rightarrow {}^3H_4$), which belong to the first and second steps of the PCE, respectively. The excitation spectra of these lines are presented in figures 2 and 3.

At room temperature the intensity of the 402 nm band of $SrAl_{12}O_{19}$:Pr (1%) begins to grow for energy of incident photons $E \geqslant 6.0$ eV (figure 2(a)), which corresponds to the onset of interconfiguration $4f^2 \rightarrow 4f5d$ transitions. The excitation edge and the known position of the $^1S_0$ level [7] (see also figure 7) allow us to find that in $SrAl_{12}O_{19}$:Pr the lowest level of the 4f5d configuration is located at $\Delta(5d,\ {}^1S_0) = 0.24$ eV above the $^1S_0$ level, yielding good conditions for PCE. The excitation spectrum in the range of $4f^2 \rightarrow 4f5d$ transitions contains a band peaked at 6.39 eV. The band also shows peculiarities at 6.2 and 7.14 eV. The threshold at $E > 7.5$ eV is certain to arise from the electronic transitions between valence and conduction bands of the host crystal. So, we can estimate the width of the forbidden band of $SrAl_{12}O_{19}$ as 7.5 eV at room temperature. The spectrum in the range from 8 to 20 eV is typical for many phosphors. One can see that the shapes of the time-integrated, slow and fast excitation spectra are similar. A feature of the fast spectrum is a relatively low emission efficiency in the range of interband transitions ($E > 7.5$ eV). Also, the intensity of the fast emission differs from zero at $E < 6.0$ eV.

For low-temperature spectra (figure 2(b)) the edge of the 4f5d configuration appears at 6.15 eV and $\Delta(5d,\ {}^1S_0) = 0.39$ eV. The excitation spectra in the range of the $4f^2 \rightarrow 4f5d$ transitions shows two main peaks at 6.27 and 6.46 eV, and a weak peak at 7.18 eV. In the pre-threshold region one can distinguish a small peak at 5.756 eV originating from $^3H_4 \rightarrow {}^1S_0$ transitions (see for details figure 7). A special feature of the low-temperature spectra of $SrAl_{12}O_{19}$:Pr is a very low intensity of the 402 nm emission at energies larger than 7.5 eV. This means that the energy transfer from the host to the activator (Pr^{3+}) is not efficient at low temperatures.

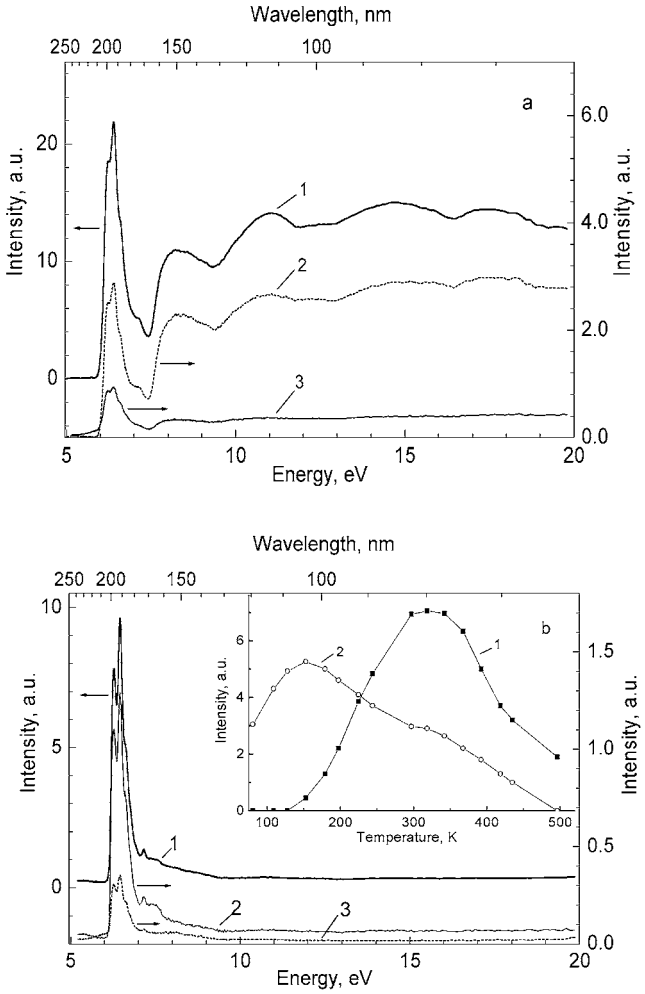

Figure 2. Excitation spectra of the 402 nm emission of $SrAl_{12}O_{19}$:Pr (1%) at: (a) 300 K and (b) 14 K; 1: time-integrated; 2: slow (100–500 ns); and 3: fast (0–5 ns) components. Inset: temperature dependences of 402 nm (1) and 486 nm (2) emission intensities.

The variations of the intensities of the x-ray-excited 402 and 486 nm lines with temperature are shown in the inset of figure 2(b). Since x-rays create free electrons and holes, it is reasonable to suppose that under band-to-band excitation the dependences will be similar. One can see that starting from room temperature the intensity of the first step in the PCE drops with decreasing of temperature and the 402 nm line almost disappears at $T < 130$ K (curve 1, inset figure 2(b)). This means that electron–hole pairs created by incident radiation do not excite the $^1S_0$ level of Pr^{3+} centres at low temperatures. Below 130 K the $^3P_0$ luminescence falls with decreasing temperature, but it retains rather high intensity at 80 K (curve 2, inset of figure 2(b)). The high-temperature ($T > 320$ K) drops of both curves in the inset of figure 2(b) are attributed to the usual thermal quenching of the luminescence.

Excitation spectra of the $^3P_0$ luminescence (486 nm line) are presented in figure 3. The positions of the first (6.0 eV) and second (7.5 eV) thresholds and main peaks for the $^3P_0$ luminescence (figure 3(a)) are the same as for $^1S_0$ luminescence (figure 2(a)). The low-temperature spectra (figure 3(b)) in the range of $4f^2 \rightarrow 4f5d$ transitions exhibit a threshold at 6.15 eV and

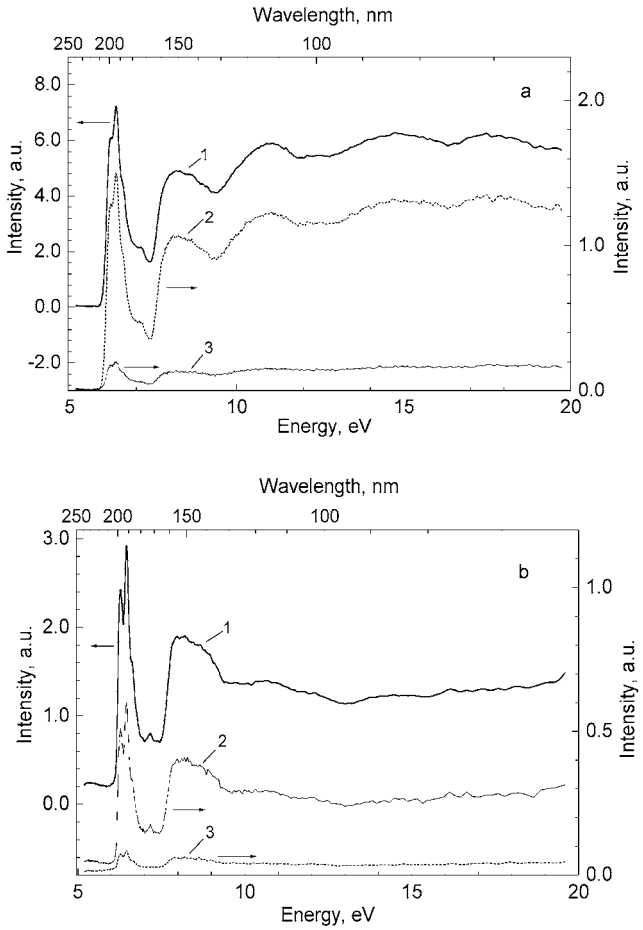

Figure 3. Excitation spectra of the 486 nm emission of $SrAl_{12}O_{19}$:Pr (1%) at: (a) 300 K and (b) 14 K; 1: time-integrated; 2: slow (100–500 ns); and 3: fast (0–5 ns) components.

peaks at 6.27 and 6.46 eV. The essential feature of the $^3P_0$ luminescence is an efficient excitation at low temperatures in the range of band-to-band transitions. The band gap of $SrAl_{12}O_{19}$, estimating from the data of figure 3(b), is 7.6 eV, i.e., slightly larger than at 300 K. Another dissimilarity from the $^1S_0$ luminescence is that the fast component of the $^3P_0$ luminescence is not excited at energies less than 6.0 eV (curves 3, figures 3(a), (b)). So, the main point is that the $^3P_0$ luminescence is excited efficiently in the region of interband transitions ($E > 7.5$ eV) at 300 K as well as at 14 K. Thus, electron–hole pairs in $SrAl_{12}O_{19}$:Pr transfer their energy to the $^3P_0$ level (figure 3(b)), but do not transfer it to $^1S_0$ level (figure 2(b)) at low temperature.

In order to study the mechanism of energy transfer from the host to different praseodymium 4f levels, the spectra of $SrAl_{12}O_{19}$ samples with low concentrations of Pr^{3+} have been measured. At 6.7 eV excitation the emission spectrum of $SrAl_{12}O_{19}$:Pr (0.1%) contains a wide band in the range 250–500 nm together with the lines arising from f–f transitions of Pr^{3+} (figure 4). This spectrum is quite similar to that observed under x-ray excitation [8]. The wide-band intrinsic luminescence with a maximum near 300 nm may be attributed to excitonic emission. This emission is suppressed in the $SrAl_{12}O_{19}$ samples containing $\geqslant$0.5 mol% of Pr^{3+} [9].

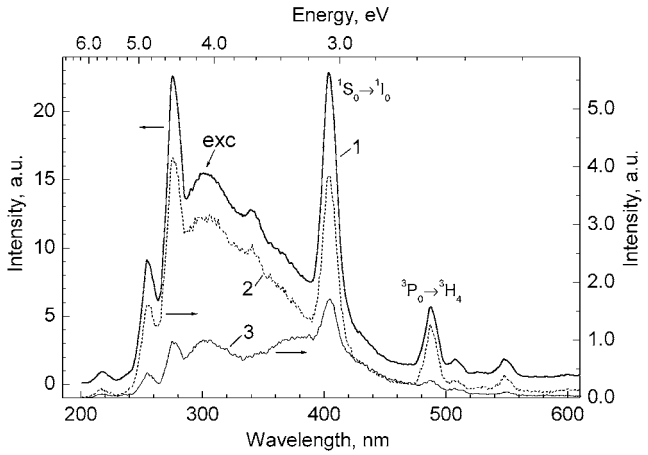

Figure 4. Emission spectra of $SrAl_{12}O_{19}$:Pr (0.1%) excited by 6.7 eV quanta: 1: time-integrated; 2: slow (10–500 ns); and 3: fast (0–5 ns) components. $T = 300$ K.

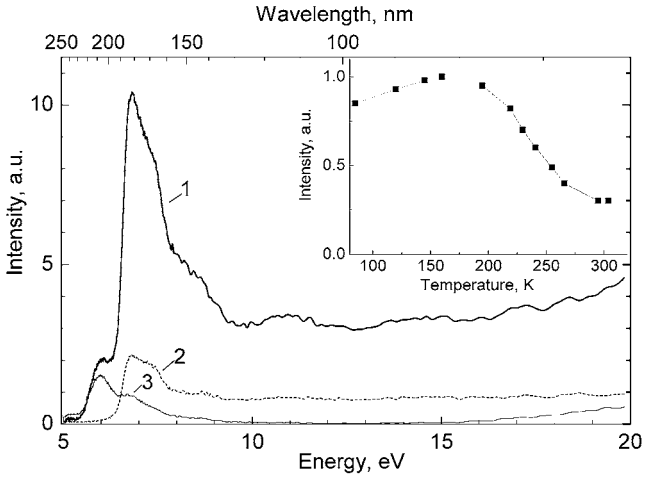

Figure 5. Excitation spectra of the 300 nm emission of $SrAl_{12}O_{19}$:Pr (0.1%): 1: time-integrated; 2: slow (100–500 ns); and 3: fast (0–5 ns) components. Inset: the temperature dependence of the 300 nm emission band intensity.

The excitation spectra of the intrinsic luminescence of $SrAl_{12}O_{19}$:Pr (0.1%) are presented in figure 5. The first threshold of the time-integrated spectra is detected at $E \geqslant 5.52$ eV with the main contribution from the fast component. The next threshold is at $E \geqslant 6.28$ eV and it arises from the slow component (curve 2, figure 5). The 300 nm band emission exhibits maximum intensity at incident quanta energy 6.82 eV. In the range of interband transitions, the efficiency of the intrinsic luminescence is rather small. Thus, the excitation spectrum of the intrinsic (excitonic) luminescence in $SrAl_{12}O_{19}$:Pr is located in almost the same energy range as $4f^2 \rightarrow 4f5d$ transitions of Pr^{3+}—that is, just below the interband transition region. The inset of figure 5 shows the intensity of the intrinsic luminescence of $SrAl_{12}O_{19}$:Pr (0.1%) as a function of temperature. The curve bears a similarity to the temperature dependence of the $^3P_0$ luminescence (curve 2, inset of figure 2(b)) and it anticorrelates with the curve for the $^1S_0$ luminescence (curve 1, inset of figure 2(b)).

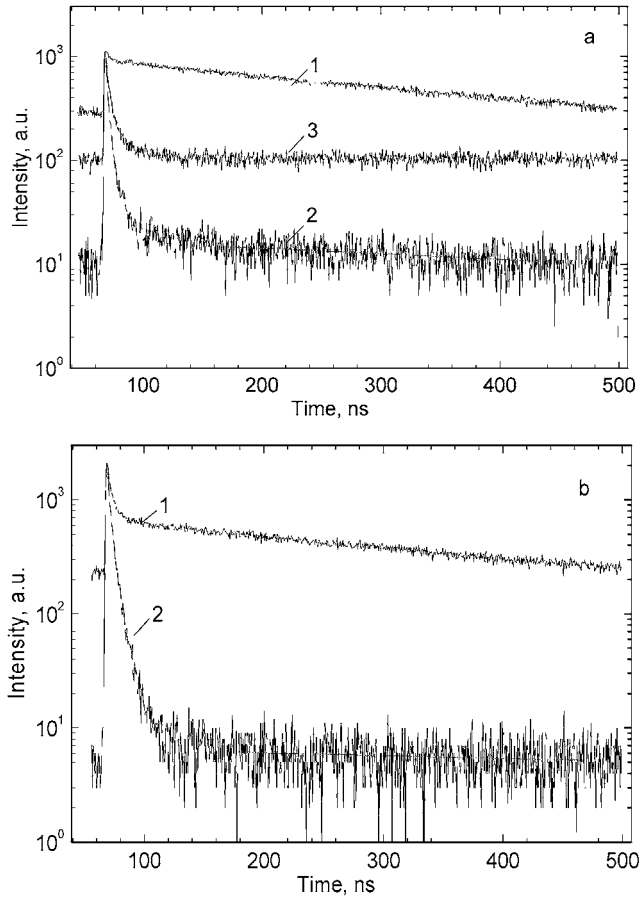

Figure 6. Decay curves recorded at 300 K for (a) $SrAl_{12}O_{19}$:Pr (1%) and (b) $SrAl_{12}O_{19}$:Pr (0.1%): 402 nm emission at 6.4 eV (1) and 5.87 eV (2) excitation; 486 nm emission at 5.87 eV excitation (3).

The excitation spectra of the $^1S_0$ and $^3P_0$ luminescences of $SrAl_{12}O_{19}$:Pr (0.1%) have been measured also. The spectra are quite similar to the appropriate spectra for $SrAl_{12}O_{19}$:Pr (1%). A feature is that the excitation spectra of the samples with low concentrations of Pr^{3+} exhibit a better spectral resolution, as is often the case.

Figure 6 presents decay curves of the main emission lines at 402 and 486 nm. In $SrAl_{12}O_{19}$:Pr (1%) at excitation near the maximum of $4f^2 \rightarrow 4f5d$ transitions (6.4 eV), the $^1S_0 \rightarrow {}^1I_6$ luminescence at 300 K exhibits exponential decay with constant $\tau = 330 \pm 10$ ns (curve 1, figure 6(a)); the contribution of the fast component is very small. At 14 K the decay constant of the $^1S_0$ luminescence is slightly larger: $\tau \approx 400$ ns, which is less than the 650 ns reported in paper [10]. The 402 nm luminescence shows fast ($\tau \approx 10$ ns) and slow ($\tau \approx 0.7$ μs) components under low-energy (5.87 eV) excitation (curve 2, figure 6(a)). It is clear that the fast component is associated with excitonic emission, because the excitation is performed in the range of the exciton creation (curve 3, figures 2 and 5). Under the same conditions, the 486 nm luminescence also contains a fast ($\tau \approx 10$ ns) and a slow ($\tau > 10$ μs) component (curve 3, figure 6(a)).

For $SrAl_{12}O_{19}$:Pr (0.1%) the main decay constant of the $^1S_0 \rightarrow {}^1I_6$ luminescence at 300 K is also 330 ± 10 ns, but the contribution of the fast component is larger (curve 1, figure 6(b))

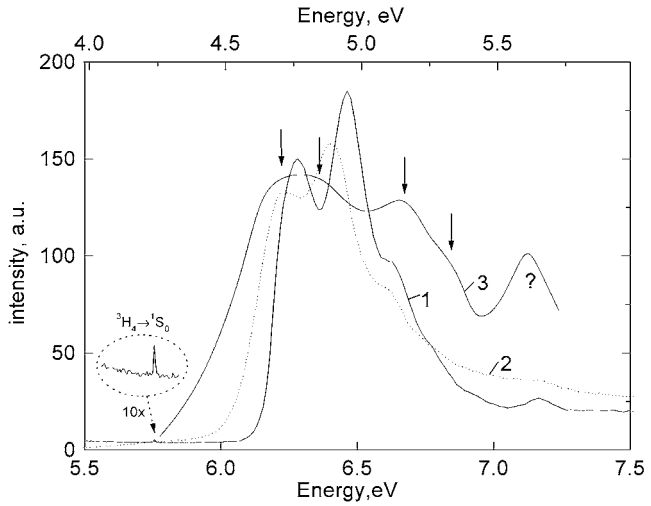

Figure 7. Excitation spectra of 402 nm emission in $SrAl_{12}O_{19}:Pr^{3+}$ (1%) at 14 K (curve 1) and in $SrAl_{12}O_{19}:Pr^{3+}$ (0.1%) at room temperature (curve 2). The region around the $^3H_4 \rightarrow {}^1S_0$ excitation in spectrum 1 has been shown on a ten-times-expanded scale. Spectrum 3 is the excitation of Ce^{3+} emission in $SrAl_{12}O_{19}$:14% Ce^{3+} at room temperature from [14]. The energy scale on the bottom axis applies to the curves 1 and 2 and the top axis to curve 3.

than in the case of $SrAl_{12}O_{19}$:Pr (1%). Excitation of the 402 nm emission in the pre-threshold region (5.87 eV) produces a very intense fast component with $\tau_1 = 11 \pm 1$ ns and a weak slow component with $\tau_2 > 1$ μs (curve 2, figure 6(b)). The wide-band (excitonic) emission (5.87 eV excitation) shows a similar profile of the decay curve with the main decay constant $\sim$10 ns.

It is well established that the 4f5d configuration of Pr^{3+} is always found at 1.52 ± 0.09 eV higher energy than the 5d configuration of Ce^{3+} [13]. Figure 7 shows the excitation spectra (curves 1, 2) for $SrAl_{12}O_{19}:Pr^{3+}$ together with the 5d excitation spectrum of Ce^{3+} in $SrAl_{12}O_{19}$ (curve 3) obtained from [14]. The arrows indicate the possible locations of the first four unresolved 5d bands of Ce^{3+}. The fifth 5d band is probably hidden somewhere under the peak of unknown origin at 5.7 eV. By shifting the energy scale of the Ce^{3+} spectrum by 1.52 eV relative to the Pr scale, the similarities between the two spectra are revealed.

4. Discussion

The most important result is that the $^1S_0$ luminescence is not detected under low-temperature band-to-band excitation (figure 2(b)). Under these conditions the Pr^{3+} luminescence occurs via a recombination mechanism. Although it can describe the low-temperature decrease of $^1S_0$ luminescence, it is difficult to explain the population of the $^3P_0$ level, while $^1S_0$ is not populated. We have to account for the participation of excitonic states in the energy transfer process.

The excitonic states in alkaline-earth and alkali halides have been well studied [15]. Across-band-gap excitation generates free holes in the valence band of the crystal, which are converted to relaxed or self-trapped holes (STHs) within about 10^{-12} s. The STHs or V_K centres in halides have been well studied. This model is also acceptable for some oxides, where they are called V_K-like centres. The STHs are mobile at room temperature via so-called hopping motion through the bulk. Some of them can reach activator centres and take part in the process of activator luminescence. In activated crystals such as NaI:Tl the hole self-trapping competes with direct trapping of holes by Tl^+ centres. At low temperatures the holes become immobile and they cannot reach the activator centres.

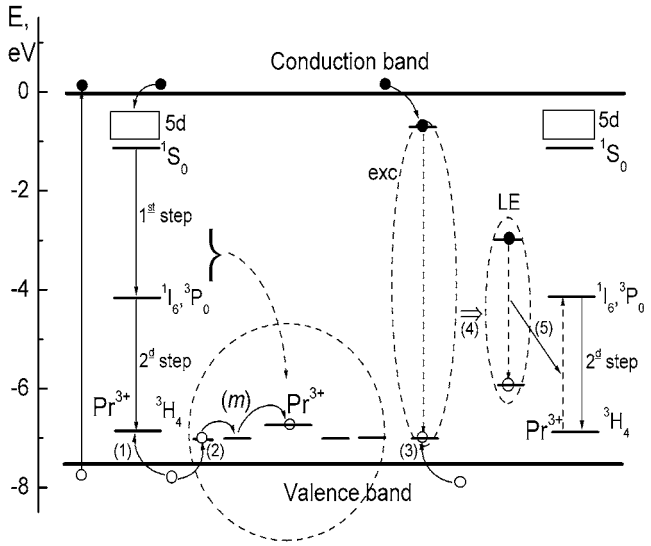

Figure 8. A schematic illustration of the different excitation, emission, and energy transfer processes in $SrAl_{12}O_{19}$:Pr^{3+}. The processes described in the text are numbered accordingly.

The STHs can capture free electrons from the conduction band, creating self-trapped excitons (STEs) which produce the excitonic luminescence. The intrinsic luminescence due to STEs was observed in many halides as well as in some oxides [15]. In many crystals this luminescence is detected only at low temperatures, but in alkaline-earth fluorides the excitonic luminescence is effective even at room temperature [15]. For some semiconductors so-called extrinsic self-trapping has been considered; it includes the intrinsic electron–lattice coupling as well as the localizing effects of a weak impurity potential [16].

Without going into details of the trapped state for holes and excitons we can apply the above model to $SrAl_{12}O_{19}$:Pr. The fact that the temperature dependences of the luminescence of $SrAl_{12}O_{19}$:Pr (inset of figure 2(b)) and another PCE phosphor $SrAlF_5$:Pr [4] are rather similar is an additional reason to use this concept. The properties of $SrAl_{12}O_{19}$:Pr are similar to those of $LaMgAl_{11}O_{19}$:Pr, which emits only a wide excitonic band peaked at 350 nm and a $^3P_0 \rightarrow {}^4H_3$ line (no $^1S_0$ luminescence) at room temperature [8]. The excitation spectra of STEs in SrF_2 [17] and intrinsic luminescence in $SrAl_{12}O_{19}$:Pr (figure 4) exhibit similar properties; in particular, the threshold of the fast component is at lower energy than that of the slow component (figure 5). Because of the similarity to physical processes in halides, we shall use in the case of the strontium aluminate the terms trapped hole (TH) and localized exciton (LE) instead of STH and STE. The origin of the centres for trapping of valence holes to TH states is unknown. It cannot be the Mg (co-activator) centres due to the variation of the emission characteristics with the concentration of Pr and correspondingly Mg. Most likely the hole trapping is an intrinsic feature of the compound creating V_K-like centres.

The model of the different processes in $SrAl_{12}O_{19}$:Pr is presented in figure 8. Let us consider band-to-band excitation where a number of electrons in the conduction band and holes in the valence band are created. Assuming that the ground state of trivalent praseodymium is above the top of the valence band, Pr^{3+} can capture a valence hole, producing Pr^{4+}. Then Pr^{4+} captures an electron from the conduction band into an excited state of Pr^{3+}, which emits light: $Pr^{4+} + e^- \rightarrow (Pr^{3+})^* \rightarrow h\nu$ (case 1, figure 8). An alternative process for the hole is trapping (or self-trapping) in a TH state; suppose that the TH is created inside a so-called 'dark sphere'

around a Pr^{3+} ion (case 2). The sphere (dotted curve) indicates a region where the probability for the TH to move towards Pr^{3+} is larger than the probability of other hole actions. At high temperature the THs are involved in the hopping motion towards Pr^{3+} '(m)' and take part in excitation of the activator. If a TH is created outside the 'dark sphere' (case 3), it can capture an electron from the conduction band creating an exciton ('exc' in figure 8). Similar excitonic states are created directly by incident quanta in the energy range from 5.52 to about 7 eV. After relaxation (case 4) the exciton (LE) can decay radiatively or transfer its energy to the activator (case 5).

At high concentration of Pr^{3+} ions ($\geqslant$0.5 mol%) the dark spheres overlap with each other and almost all holes are captured by Pr^{3+} ions. As a result, the excitonic emission is not detected in highly concentrated samples (see, e.g., figure 1). At low concentration of Pr^{3+} ions (<0.5%) some holes are created outside the spheres producing excitonic states (case 3) and excitonic luminescence (figure 4).

The intensity of the $^1S_0$ luminescence decreases (curve 1, inset figure 2(b)) with decreasing temperature due to the reduction in TH mobility. At low temperature (<130 K for $SrAl_{12}O_{19}$:Pr) the THs become stable (immobile) and cannot reach Pr^{3+} centres; correspondingly the process $3 \rightarrow 4 \rightarrow 5$ prevails (figure 8), while the intensity of $^1S_0$ luminescence becomes negligible. The absence of the $^1S_0$ luminescence at low temperature under across-band-gap excitation indicates that the Pr^{3+} states are fed basically from THs and not from free valence holes.

The $^3P_0$ luminescence retains high intensity at low temperatures due to energy transfer from LE to Pr^{3+} centres (case 5). The LEs have enough energy for population of the $^3P_0$ level, but not enough for feeding the $^1S_0$ level. Note that a similar mechanism of energy transfer from host crystal to Pr^{3+} has been proposed for $SrAlF_5$:Pr [4] and LaF_3:Pr [18].

The emission decay curves have been measured in the range 0–500 ns (figure 6) and obviously the slow components of f–f transitions of Pr^{3+} fall beyond this range. We will use the term 'slow component' for decays of several hundred nanoseconds. The slow 300 ns emission for $4f^2 \rightarrow 4f5d$ excitation (6.4 eV) can arise due to mixing of 5d and 4f states [11]; the fast component of the $^1S_0$ luminescence is almost negligible in $SrAl_{12}O_{19}$:Pr (1%) (curve 1, figure 6(a)). The fast component appears for pre-threshold ($E < 6.0$ eV) excitation of $^1S_0$ and $^3P_0$ luminescence (curves 2, 3 in figure 6). It is clear that this component is related to fast emission of the LEs. These excitons are created also with interband excitation but the contribution of their emission to the total light output is not large.

A comparison of the excitation spectra of Pr^{3+} and known data for Ce^{3+} in $SrAl_{12}O_{19}$ (figure 7) allows us to state the following conclusions. Ignoring any interaction between 5d and 4f electrons in the 4f5d configuration of Pr^{3+}, the 5d electron will experience the same crystal field splitting and shift as in Ce^{3+}. The electron remaining in the 4f orbital may occupy the $^2F_{5/2}$ ground state but also the $^2F_{7/2}$ excited state. This means that the main splitting of the 4f5d configuration of Pr^{3+} is the same as that of Ce^{3+}. In addition the 4f5d spectrum of Pr^{3+} will show substructure due to the different levels occupied by the 4f electron. For a more detailed discussion that also includes the interactions between 4f and 5d electrons we refer the reader to [19]. The total crystal field splitting is less than 1 eV for Pr^{3+} as well as for Ce^{3+} in $SrAl_{12}O_{19}$, which is amongst the smallest encountered in inorganic compounds [5]. This is the main reason for the relatively large value of $\Delta E(5d, {}^1S_0) = 0.39$ eV that makes the cascade emission possible.

5. Conclusions

At $4f^2 \rightarrow 4f5d$ excitation (6.7 eV), the emission spectrum of $SrAl_{12}O_{19}$:Pr measured at 14 K shows a number of lines originating from the $^1S_0$ and $^3P_0$ multiplets of Pr^{3+} ions and this

spectrum is similar to that at room temperature. The excitation of the $^1S_0 \rightarrow {}^1I_6$ and $^3P_0 \rightarrow {}^3H_4$ emissions occurs in a 1 eV wide region originating from the interconfiguration $4f^2 \rightarrow 4f5d$ transitions with threshold (onset of the transitions) at 6.0 eV at room temperature and at 6.15 eV at 14 K. The excitation band contains two main peaks at 6.27 and 6.46 eV and a weak peak at 7.18 eV, which are resolved well particularly at low temperature. The next threshold in the excitation spectrum near 7.5 eV corresponds to the transitions from the valence to the conduction band. The excitation peak originating from $^3H_4 \rightarrow {}^1S_0$ transitions is located at 5.756 eV. A comparison of the excitation spectra of Pr^{3+} and Ce^{3+} in $SrAl_{12}O_{19}$ reveals the shift of 1.52 eV between the 5d states of the ions. So, $SrAl_{12}O_{19}$ provides another example showing that the model developed in [5] applies well.

At band-to-band excitation ($E > 7.5$ eV) and at low temperatures, the luminescence from the $^3P_0$ level is excited efficiently while $^1S_0$ luminescence is absent. To explain this, a mechanism involving the valence hole trapping and transfer of the energy from excitonic states to Pr^{3+} ions is proposed.

Decay time constants for the main emission lines of Pr^{3+} have been measured. At excitation near the maximum of $4f^2 \rightarrow 4f5d$ transitions (6.4 eV), the $^1S_0 \rightarrow {}^1I_6$ luminescence exhibits exponential decay with constant $\tau = 330 \pm 10$ ns at 300 K and $\tau \approx 400$ ns at 14 K. At pre-threshold excitation ($E < 6.0$ eV) a fast component $\tau \approx 10$ ns originating from excitonic emission prevails.

Acknowledgments

This work was supported by the Russian Foundation for Basic Research, project No 01-02-17960, INTAS Grant No 99-01350 and the Dutch Technology Foundation (STW). The support and hospitality of Professor G Zimmerer and Dr M Kirm are also gratefully acknowledged.

References

[1] Shionoya S and Yen W M (ed) 1995 *Phosphor Handbook* (London: Chemical Rubber Company Press) ch 10
[2] Merkle L D, Zandi B, Moncorge R, Guyot Y, Verdun H R and McIntosh B 1996 *J. Appl. Phys.* **79** 1849
[3] Lindop A J, Metthews C and Goodwin D W 1975 *Acta Crystallogr.* B **31** 2940
[4] Vink A P, Dorenbos P, de Haas J T M, Donker H, Rodnyi P A, Avanesov A G and van Eijk C W E 2002 *J. Phys.: Condens. Matter* **14** 8889
[5] Dorenbos P 2002 *J. Lumin.* **99** 283
[6] Srivastava A M and Beers W W 1997 *J. Lumin.* **71** 285
[7] Huang S, Lu L, Jia W, Wang X, Yen W M, Srivastava A M and Setlur A A 2001 *Chem. Phys. Lett.* **348** 11
[8] Rodnyi P A, Mikhrin S B, Dorenbos P, van der Kolk E, van Eijk C W E, Vink A P and Avanesov A G 2002 *Opt. Commun.* **204** 257
[9] Rodnyi P A, van Eijk C W E, Mishin A N, Mikhrin S B, Avanesov A G and Potapov A S 2002 *Proc. SPIE* **4766** 165
[10] Huang S, Wang X, Meltzer R S, Srivastava A M, Setlur A A and Yen W M 2001 *J. Lumin.* **94/95** 119
[11] Zandi B, Merkle L D, Gruber J B, Wortman D E and Morrison C A 1997 *J. Appl. Phys.* **81** 1047
[12] Zimmerer G 1991 *Nucl. Instrum. Methods Phys. Res.* A **308** 178
[13] Dorenbos P 2000 *J. Lumin.* **91** 155
[14] Stevels A L N 1978 *J. Electrochem. Soc.: Solid State Sci. Technol.* **125** 588
[15] Williams R T and Song K S 1990 *J. Phys. Chem. Solids* **51** 679
[16] Toyazawa Y 1990 *Rev. Solid State Sci.* **4** 133
[17] Aleksandrov Yu M, Makhov V N, Rodnyi P A, Syreishchikova T I and Yakimenko M N 1986 *Sov. Phys.–Solid State* **28** 1598
[18] Srivastava A M and Duclos S J 1997 *Chem. Phys. Lett.* **275** 453
[19] Van Pieterson L, Reid M F, Wegh R T, Soverna S and Meijerink A 2002 *Phys. Rev.* B **65** 045113